GEOPHYSICAL RESEARCH LETTERS, VOL. 28, NO. 21, PAGES 4151-4154, NOVEMBER 1, 2001

# Interannual Upper Ocean Variability in the Tropical Indian Ocean

Ming Feng, Gary Meyers, and Susan Wijffels

CSIRO Marine Research, Hobart, Tasmania, Australia

**Abstract.** Empirical orthogonal function (EOF) analysis is used to characterize interannual upper ocean temperature variability since mid-1980s along two repeated XBT sections across the Indian Ocean. The mode 1 EOF loadings have deepened thermocline in the western tropical Indian Ocean and a shoal thermocline in the east/southeast Indian Ocean during the 1994 and 1997/98 Indian Ocean dipole (IOD) events. Reversed anomalies occur during 1988/89, 1996, and 1998/99. The mode 2 EOF loadings only have significant magnitudes related to the IOD, with upwelling (downwelling) along the Sumatra-Java coast and downwelling (upwelling) in the southern subtropics leading (lagging) the IOD peaks. Lagged correlations between sea level anomaly and westward wind stress anomaly along the equatorial Indian Ocean (an IOD index) support the EOF analysis: the two EOF modes are linked by propagation and reflection of subtropical Rossby waves and equatorial Kelvin waves, which also contribute to reverse the IOD through a delayed action.

## Introduction

An Indian Ocean dipole (IOD) event is characterized by sea surface temperature (SST) anomalies in the tropical Indian Ocean where warmer than usual SSTs occur over large parts of the western basin and cooler SSTs off Sumatra in the east basin (*Saji et al.*, 1999). The normal equatorial westerly winds are weakened and reverse direction during the boreal summer of an IOD event. The IOD influences regional climate and has attracted interest in recent years, especially the 1994 (*Behera et al.*, 1999; *Vinayachandran et al.*, 1999) and 1997/98 events (*Yu and Rienecker*, 1999; *Webster et al.*, 1999).

Statistically, El Nino/Southern Oscillation (ENSO) has a substantial impact on interannual variability of the Indian Ocean (*Tourre and White,* 1995; *Reason et al.,* 2000). However, both observations (*Webster et al.*, 1999; *Saji et al.*, 1999) and models (*Iizuka et al.*, 2000) suggest that the Indian Ocean also has its own interannual air-sea coupled mode. *Vinayachandran et al.* (2000) pointed out the existence of both positive and negative IOD events.

With the development of the ENSO observing network in the Pacific, ENSO theory (Neelin et al., 1998) and ENSO predictability (Latif et al., 1998) have been greatly improved. However, a comparable understanding of the coupled dynamics in the Indian Ocean is lacking. The present study uses upper ocean temperature and satellite altimeter data to characterize the upper ocean evolution related to the IOD events.



Paper number 2001GL013475.
0094-8276/01/2001GL013475$05.00

## Data and Methods

The Expendable Bathythermograph (XBT) temperature data were collected by a Ship of Opportunity network in the Indian Ocean, of which we use two frequently repeated lines (Fig. 1): IX1 from Fremantle, Australia to Sunda Strait, Indonesia, and IX12 from Fremantle to the Red Sea (*Meyers and Pigot*, 1999). The XBT data were binned by latitude and optimally interpolated in time to monthly values. By subtracting the mean annual cycle and applying a five-month moving average and then a five-point hanning filter in time, the interannual ocean temperature anomaly in the upper 440 m from 1986 to 1999 is obtained. The temperature data are normalized at each grid point, before a joint empirical orthogonal function (EOF) analysis is applied to the combined data from both sections. To recover physical units, the EOF loadings are multiplied by the interannual temperature standard deviations before being plotted.

A 10 day/0.25 degree gridded altimeter sea level anomaly (SLA) product based on the combined TOPEX Poseidon and ERS-1/ERS-2 missions from October 1992 to end of 1999 was obtained from CLS Space Oceanography Division (*Le Traon et al.,* 1998). A one-degree resolution subset of the data is used here. Annual and semi-annual harmonics are calculated by linear regression and are subtracted to obtain the interannual SLA. The data are further smoothed in time similar to the XBT data and in space with a nine-point average.

Other data used in the present study include: the Southern Oscillation Index (SOI) obtained from the Bureau of Meteorology, Australia; National Centers for Environmental Prediction (NCEP) reanalysis wind stress data; European

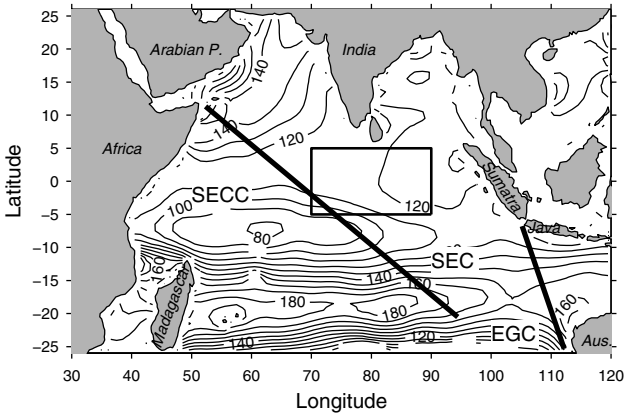


**Figure 1.** Annual mean 20°C isotherm depth in the Indian Ocean (*Levitus and Boyer,* 1994). The heavy lines denote the IX1 and IX12 XBT lines. The solid box denotes the region used to define the wind stress IOD Index (see text).

Space Agency Remote Sensing Satellite (ERS) scatterometer wind stress data from 1991 obtained from IFREMER, France; and the *Levitus and Boyer* (1994) ocean temperature climatology. The SOI and interannual wind stress anomalies are smoothed in time the same as the XBT data.

## Interannual Temperature Variability From EOF Analysis

The annual mean 20°C isotherm depth largely represents the mean upper ocean circulation pattern in the tropical Indian Ocean (Fig. 1). There is a pronounced zonal ridge along 7°S west of 90° E, supporting the westward flowing South Equatorial Current (SEC) to its south and the South Equatorial Counter Current (SECC) to its north. The SEC is joined by the Indonesian Throughflow from gaps between the Indonesian island chain and Australia. The thermocline trough along 20°S separates the SEC from the eastward East Gyral Current which feeds the southward Leeuwin Current along the West Australian coast. In the northern Indian Ocean, the mean circulation is weak because of the annual reversal of the monsoonal winds. Salient features are the northeastward East Arabian Coastal Current/Somali Current and their return flows in the Arabian Sea. The IX1 line cuts through the Indonesian Throughflow/SEC system, and is influenced by the equatorial Indian Ocean at its northern end and by Pacific signals at its southern end, through the coastal wave guides (*Meyers*, 1996). The IX12 line intersects the SEC ridge/trough structure in the southern Indian Ocean, crosses the equatorial wave guide and the boundary currents at the African coast.

The first joint EOF (EOF-1) of the temperature anomaly explains 19% of the total interannual temperature variance, while the second EOF (EOF-2) explains 12%. EOF-1 loadings are mostly negative along IX1, with a peak value of -1.2° C at 80 m near the Sumatra-Java coast (Fig. 2a). South of 20°S, loadings are largely -0.2 to -0.3°C. Converting temperature loadings into isothermal depth displacements using the mean vertical temperature gradients, the largest displacement occurs near the Australian coast due to the weaker stratification there (*Meyers*, 1996).

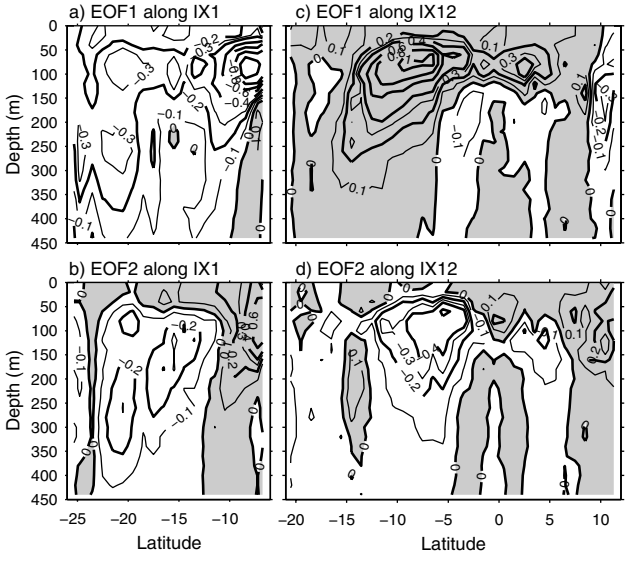


**Figure 2.** Joint EOF-1 and EOF-2 loadings along the IX1 (a and b) and IX12 (c and d) XBT lines. The loadings have been multiplied by the interannual temperature standard deviations. Grey shading denotes positive loadings. The unit is °C.

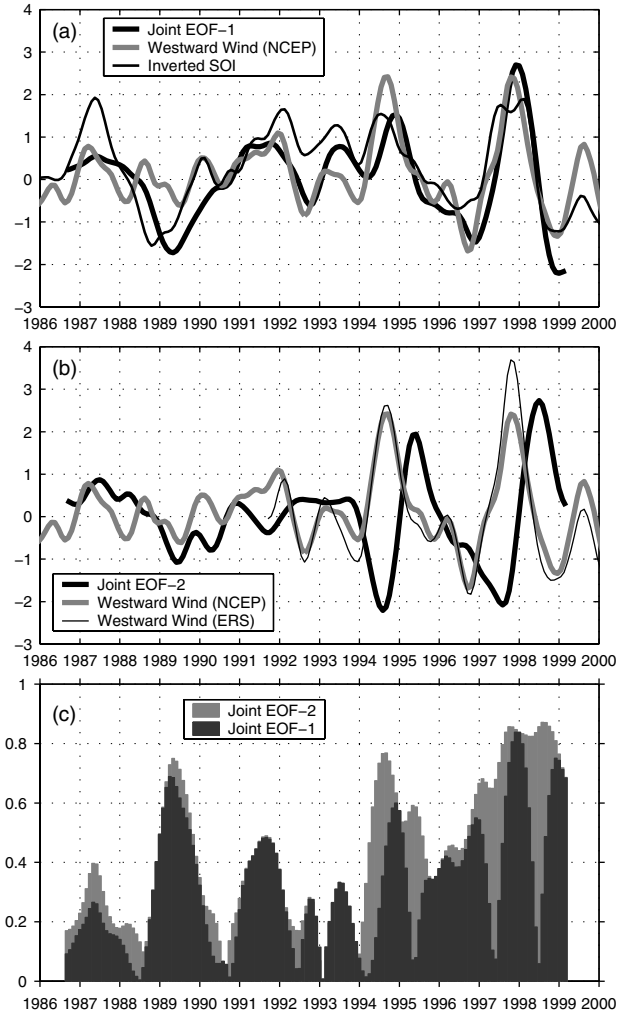


**Figure 3.** Time coefficients of (a) EOF-1 and (b) EOF-2 and their comparisons with inverted SOI and average equatorial Indian Ocean westward wind stress anomalies (unit: 0.01 Pa), and (c) correlations between observed and EOF reconstructed fields.

The EOF-1 loadings along IX12 are dominantly positive in the upper ocean, with peak value of 1°C at 80 m centered around 6-10°S (Fig. 2c), coinciding with the ridge between the SEC and SECC, where the shallow thermocline depth changes may have an impact on the mixed layer heat budget. Near 2–3°N, there is a 0.4°C local maximum at similar depths. Negative loadings occur immediately off the African coast, which are associated with stronger coastal currents.

The IOD can be indexed with the westward wind stress anomalies within 70–90°E, 5°S–5°N box (Figs. 1 and 3), which are well correlated with zonal equatorial SST gradient anomalies (not shown). Here we define an IOD peak as a maximum westward wind anomaly, such as occurred in August–September 1994 and October 1997. Significant positive EOF-1 time coefficients (larger than one standard deviation) occur during the 1994 and 1997/98 IOD events (Fig. 3a), that is, with deepened thermocline

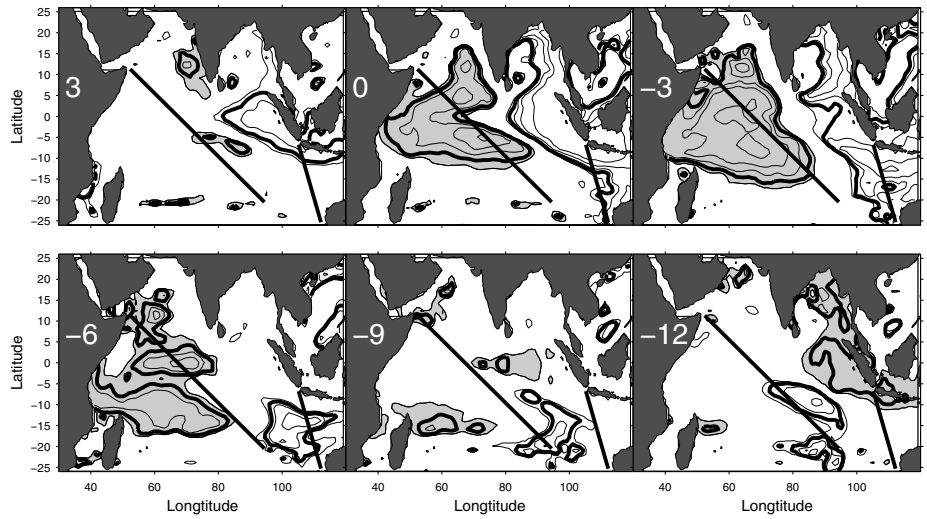


**Figure 4.** Lagged correlations between altimeter SLA and equatorial westward wind stress anomalies. Numbers in the panels denote months that SLA leads the wind anomaly. Positive correlations are shaded, and only correlations larger than 0.5 are contoured with an increment interval of 0.1. The heavy contours are 0.6. The locations of the XBT lines are denoted.

in the west tropical Indian Ocean and shoal thermocline in the east/southeast Indian Ocean. During the 1988/89 and 1998/99 La Nina, and the 1996 negative IOD event (Vinayachandran et al., 2000), EOF-1 has negative anomalies. Note that the subsurface signals during the 1986/87 and 1991/92 El Nino events are not significant. EOF-1 varies closely with the IOD wind index during the large 1994 and 1997/98 IOD events, and the 1996 negative IOD event, with peak magnitude in November 1994 and December 1997, lagging the IOD peak by 2-3 months.

In the thermocline along IX1, EOF-2 has negative loadings south of 12°S, the approximate location of the SEC front, and positive loadings in the north near the Sumatra-Java coast (Fig. 2b). The surface layer loadings are mostly positive. The main feature of EOF-2 along IX12 is the negative loadings between 5-10°S and near 5°N centered at 80 m, and positive loadings in between at the equator (Fig. 2d).

The time coefficients of EOF-2 (Fig. 3b) only have significant magnitudes related to the 1994 and 1997/98 IOD events, with negative values leading the IOD peaks, and positive values after the IOD peaks. That is, upwelling along Sumatra-Java and downwelling in the southern subtropics, the negative EOF-2 peaks in July–August 1994 and July–August 1997, lead the IOD peaks, while downwelling along Sumatra-Java coast and upwelling in the southern subtropics, the positive EOF-2 peaks in May 1995 and June-July 1998, lag the IOD peaks. Thus, the negative EOF-2 leads the EOF-1 by 4-5 months and the positive EOF-2 lags the EOF-1 by 6-7 months during the IOD, and the lead-lag relationships between EOF-1 and EOF-2 could be linked by the propagation and reflection of subtropical Rossby waves and equatorial Kelvin waves, as shown in the next section.

Following *Lau and Wu* (1999), we calculate spatial correlations between the observed and EOF-reconstructed temperature anomaly fields to reveal how much spatial variance the first two EOFs account for over time (Fig. 3c). EOF-1 contributes significantly during most ENSO and IOD events, except the 1986/87 and 1991/92 El Nino events. EOF-2 contributes significantly before and after the 1994 and 1997/98 IOD peaks (higher than 0.5), and is only on the order of 0.1 at other times. Thus, EOF-2 can be regarded as a transition mode for the IOD.

## Lag Correlations between SLA and IOD

To further clarify the relationship between the two EOFs, we present lagged correlations between the ERS westward equatorial wind stress anomaly and altimeter SLA, which is predominantly determined by the thermocline depth in the tropical oceans. On average, correlations higher than 0.6 are significant at the 95% level. The ERS wind stress anomalies are correlated with the NCEP anomalies at 0.95, except being 50% larger during the 1997/98 IOD event (Fig. 3b).

Three months leading the wind anomaly, a correlation structure consistent with a negative temperature EOF-2 appears in the southeast Indian Ocean, with negative correlations along equator and Sumatra-Java coasts and positive correlations in the mid-South Indian Ocean (Fig. 4). Small area of positive correlation exists at the west coast of the Indian sub-continent. The negative correlations expand into the eastern Indian Ocean with time, and at zero lag are generally higher than 0.9 near the coast. The expansion follows the pattern of equatorial and coastal Kelvin waves and Rossby wave reflection at higher latitudes. The positive correlations intensify and move westward like planetary Rossby waves from 3-months lead to 3-months lag. There is a west-east dipole correlation structure during zero to 3-months time lag (consistent with EOF-1), with the east pole peaking at zero time lag and the west pole peaking at 3-month lag. *Iizuka et al.* (2000) found a similar lag correlation pattern in a heat budget analysis of a coupled model.

The westward propagating branch of the positive correlations appears to reflect into equatorial Kelvin wave and move eastward along the equator from 3-months to 12-months lag, though at speeds slower than linear free waves. When reaching the eastern boundary, the positive correlations and the reflected negative correlations form the structure consistent with positive temperature EOF-2 at a 12-months lag, reversing the IOD through a delayed action. There are slower westward propagating Rossby waves at higher

latitudes northeast of Madagascar and east of the Arabian Peninsula at 6-9 month lag, which influence the boundary current regions.

## Discussion

Enhanced southeast monsoon winds along the Sumatra-Java coast during boreal spring-summer are precursors of an IOD (*Vinayachandran et al.*, 1999; *Webster et al.,* 1999). The wind anomalies cause anomalous upwelling along the Sumatra-Java coast, and upper ocean convergence in the southern subtropical Indian Ocean (the negative EOF-2 structure). Westward propagation of the convergence, representing interannual ocean memory (*Neelin et al.,* 1998), was observed during the evolution of the 1994 and 1997/98 IOD events (*Chambers et al.,* 1999; *Webster et al.,* 1999). The Rossby waves further strengthen the SST anomaly in the western equatorial region (*Rao et al.*, 2001; *S.-P. Xie*, personal communication), causing the western Indian Ocean anomaly to peak at about 3-months lag. Thus, the subtropical Rossby waves are likely to contribute to the unstable coupled ocean-atmosphere mode in the Indian Ocean.

Eastward propagation of a deep thermocline along the equator after an IOD peak may be mainly responsible for the reversal of the event, similar to the delayed oscillator mechanism in the Pacific (*Schopf and Suarez,* 1988). The slow eastward propagation is also shown in long-term model runs (*Rao et al.*, 2001) and likely involves a coupled air-sea mode.

**Acknowledgments.** This work was supported by a special executive grant from CSIRO, Australia. We would thank Lidia Pigot for processing the XBT data and Neil White for preparing the altimeter data. We thank Tara Ansell, Andreas Schiller, P. N. Vinayachandran, and one reviewer for helpful comments. The altimeter products were produced by the French CLS Space Oceanography Division.

## References

Behera, S. K., R. Krishnan, and T. Yamagata, Unusual ocean-atmosphere conditions in the tropical Indian Ocean during 1994, *Geophys. Res. Lett., 26,* 3001-3004, 1999.

Chambers, D. P., B. D. Tapley, and R. H. Steward, Anomalous warming in the Indian Ocean consistent with El Nino, *J. Geophys. Res., 104,* 3035-3047, 1999.

Iizuka, S., T. Matsuura, and T. Yamagata, The Indian Ocean SST dipole simulated in a coupled general circulation model, *Geophys. Res. Lett., 27,* 3369–3372, 2000.

Latif, M., D. Anderson, T. Barnett, M. Cane, R. Kleeman, A. Leetmaa, J. O'Brien, A. Rosati, and E. Schneider, A review of the predictability and prediction of ENSO, *J. Geophys. Res., 101,* 14,375-14,393, 1998.

Lau, K. M., and H. -T. Wu, Assessment of the impacts of the 1997-98 El Nino on the Asian-Australia Monsoon, *Geophys. Res. Lett., 26,* 1747-1750, 1999.

Le Traon, P. Y., F. Nadal, and N. Ducet, An improved mapping method of multi-satellite altimeter data, *J. Atm. Ocean. Techn., 25,* 522-534, 1998.

Levitus, S., and T. P. Boyer, World Ocean Atlas 1994 Volume 4: Temperature, *NOAA Atlas NESDIS 4,* 117 pp., U.S. Department of Commerce, Washington, D.C., U.S.A., 1994.

Meyers, G., Variation of Indonesian throughflow and the El Nino-Southern Oscillation, *J. Geophys. Res., 101,* 12,255-12,563, 1996.

Meyers, G., and L. Pigot, Analysis of frequently repeated XBT lines in the Indian Ocean, *CSIRO Marine Laboratories Report 238,* 43 pp., CSIRO Division of Marine Research, Hobart, Australia, 1999.

Neelin, J. D., D. S. Battisti, A. C. Hirst, F. -F. Jin, Y. Wakata, T. Yamagata, and S. E. Zebiak, ENSO theory, *J. Geophys. Res., 103,* 14,261-14,290, 1998.

Rao, S. A., S. K. Behera, Y. Masumoto, and T. Yamagata, Interannual subsurface variability in the tropical Indian Ocean, *Deep Sea Res. II,* 2001 (submitted).

Reason, C. J. C., R. J. Allan, J. A. Lindesay, T. J. Ansell, ENSO and climatic signals across the Indian Ocean basin in the global context: Part 1, interannual composite patterns, *Int. J. Climatol., 20,* 1285-1327, 2000.

Saji, N. H., B. N. Goswami, P. N. Vinayachandran, and T. Yamagata, A dipole mode in the tropical Indian Ocean, *Nature, 401,* 361-363, 1999.

Schopf, P. S., and J. Suarez, On equatorial dynamics, mixed layer physics and sea surface temperature, *J. Phys. Oceanogr., 13,* 549-566, 1988.

Tourre, Y. M., and W. B. White, ENSO signals in global upper-ocean temperature, *J. Phys. Oceanogr., 25,* 1317-1332, 1995.

Vinayachandran, P. N., N. H. Saji, and T. Yamagata, Response of the equatorial Indian Ocean to an unusual wind event during 1994, *Geophys. Res. Lett., 26,* 1613-1616, 1999.

Vinayachandran, P. N., S. Iizuka, and T. Yamagata, Indian Ocean dipole mode events in an ocean general circulation model, *Deep Sea Res.,* in press, 2000.

Webster, P. J., A. Moore, J. Loschnigg, and R. Leben, Coupled ocean-atmosphere dynamics in the Indian Ocean during 1997-1998, *Nature, 401,* 356-360, 1999.

Yu, L., and M. Rienecker, Mechanisms for the Indian Ocean warming during the 1997-98 El Nino, *Geophys. Res. Lett., 26,* 735-738, 1999.

Ming Feng, Gary Meyers, and Susan Wijffels, CSIRO Marine Research, Castray Esplanade, Hobart, TAS 7001, Australia. (e-mail: ming.feng@marine.csiro.au; meyers@marine.csiro.au; wijffels@marine.csiro.au)

(Received May 21, 2001, accepted August 2, 2001.)